Continuum Mech. Thermodyn. (2023) 35:2193–2205
https://doi.org/10.1007/s00161-023-01241-9

ORIGINAL ARTICLE

Olgierd Goroch · Zbigniew Gulbinowicz · Mariusz Magier · Ewa Bednarczyk · Paweł Skoczylas · Zygmunt Pankowski · Pawel Sweklej · Pawel Zochowski · Wieslaw Jedrzejewski

Development and experimental verification of the new WHA sinters intended for kinetic energy projectiles

Received: 20 January 2023 / Accepted: 27 June 2023 / Published online: 11 July 2023

Abstract Depleted uranium (DU) and tungsten heavy alloys (WHA) are commonly used as kinetic energy projectiles penetrators due to their excellent properties such as remarkably high density and strength which significantly affect their armor penetration capabilities. This article presents the results of laboratory and field tests of the new WHA sinter which summarize the results of a development project intended to increase the strength of the above-mentioned sinters used in the production of kinetic ammunition. The alloy with the composition W91–6Ni–3Co was used for the tests. The obtained alloy was subjected to cold swaging deformation with reduction of 25%. The parameters of individual technological processes were determined based on previous research. These studies concerned the impact of the degree of cold swaging deformation on the mechanical properties of the 91W–6Ni–3Co alloy. The above-mentioned work presents the results of UTS test, Charpy impact strength measurement, hardness and microhardness measurement, and the results of WHA microscopic observations in two states: after heat treatment and the final state after cold swaging deformation

Communicated by Andreas Öchsner.

O. Goroch · Z. Gulbinowicz · M. Magier (✉) · E. Bednarczyk · P. Skoczylas
Institute of Mechanics and Printing, Faculty of Mechanical and Industrial Engineering, Warsaw University of Technology, Narbutta 85, 02-524 Warsaw, Poland
E-mail: mariusz.magier@pw.edu.pl

O. Goroch
E-mail: olgierd.goroch@pw.edu.pl

Z. Gulbinowicz
E-mail: zbigniew.gulbinowicz@pw.edu.pl

E. Bednarczyk
E-mail: ewa.bednarczyk@pw.edu.pl

P. Skoczylas
E-mail: pawel.skoczylas@pw.edu.pl

P. Sweklej · P. Zochowski
Military Institute of Armament Technology, Prym. S. Wyszynskiego 7, 05-220 Zielonka, Poland
E-mail: sweklejp@witu.mil.pl

P. Zochowski
E-mail: zochowskip@witu.mil.pl

W. Jedrzejewski
Zakłady Metalowe MESKO S.A., Legionów 122, 26-111 Skarżysko-Kamienna, Poland
E-mail: w.jedrzejewski@mesko.com.pl

with reduction of: 25%. The next purpose of the research was to check the strength and functioning of the new WHA rods used in 120 mm sub-caliber projectiles. This examination was crucial for the completion of this research project, and its results enabled a synthesis of laboratory results and experimental tests.

Keywords Tungsten sinters · Mechanical properties · Penetrator · Kinetic energy projectile

1 Introduction

Sub-caliber kinetic energy ammunition for smooth bore guns was developed to increase penetration capability of battle tanks armors. The high ability to penetrate the armor is influenced, among others, by muzzle velocity (even up to 1800 m/s), high kinetic energy of the projectile (7–8 MJ), large ratio of its length to diameter (l/d ratio is about 30), affecting a small decrease in the projectile's velocity along the flight path (about 50–60 m/s at 1000 m distance).

In the 1960s, the kinetic energy penetrators was made by using steel's alloys with excellent mechanical properties. In the 1970s, the first steel penetrators with carbide–tungsten plugs were developed. Further development of sintering processes (with additives as nickel, iron, cobalt, copper and rhenium) and improvement of the forging process of tungsten sinters made it possible to obtain longer and longer penetrators in the production process (slenderness ratio from 10 to above 30) (Fig. 1).

Tungsten heavy alloys achieve excellent mechanical properties such as strength, plasticity and tensile strength in Charpy test over a wide temperature range. The basic method of producing WHA is powder metallurgy using sintering with the participation of the liquid phase [1–3]—the reason is the high melting point of tungsten. A standard microstructure of WHA consists of hard, spheroidal, chemically pure tungsten grains with a size of $20 \div 60$ μm and a matrix called the binding phase. Due to the characteristic microstructure and the presence of at least two phases with significantly different properties, WHA are often referred to as tungsten composites [3–5]. The matrix of the alloy is a nickel-based solid solution. It contains dissolved tungsten and other alloy additives, i.e., Fe, Co, Cu, Re, Ta and Mo [4–6]. Nickel as the basic matrix component ensures the wettability and solubility of tungsten and other alloy components in the liquid phase and reduce the sintering temperature from 3420 °C for pure tungsten to about 1520 °C for the W–Ni alloy. Tungsten increases the strength of the W–matrix grain boundary and increases the thermal resistance of the alloy. The tungsten content in the Ni–W double alloy is 31% (by weight) [7], and in the three- and multi-component alloys, it depends on the quantity and quality of the alloying elements, reaching even 50% (by weight).

Depending on the intended use and related mechanical properties, tungsten heavy alloys contain $90 \div 98\%$ of tungsten, and their density is in the range of $17.0 \div 18.6$ g / cm^3.

WHA, due to its advantages, i.e., remarkably high density, favorable mechanical properties, high hardness, ease of cutting and machining, susceptibility to plastic and finishing work, have found wide application in many industries [5,6,8]. They are used, inter alia, as balancing elements in airplanes, including weights for balancing the blades of airplanes and helicopters. They are used to produce extrusion dies, elements of casting

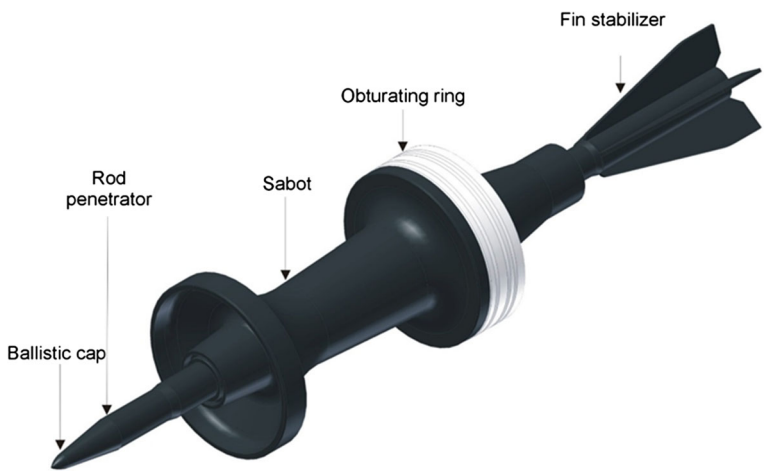

Fig. 1 Main elements of the APFSDS-T projectile

molds, vibration damping devices, gyroscopic elements, as well as vibration elements in mobile phones [9–12]. Among the numerous applications of WHA, they are used for radiation shields, collimators, isotope syringe shields, as well as in the production of EDM electrodes or contacts operating under high load [5,8,13]. WHA found a special application in the defense industry to produce sub-caliber anti-tank projectile's rods as a substitute for depleted uranium [14–21].

The basic methods of increasing of the mechanical properties of WHA are based on heat treatment and plastic working, in particular cold swaging [22–26]. Post-sintering heat treatment is conducted to improve the strength, plasticity and tensile strength in Charpy test of the WHA. The treatment is conducted in the temperature range of 1000 ÷ 1200 °C for 1–24 h in nitrogen, argon or vacuum atmosphere with cooling in water or oil. The temperature and time of annealing should be selected to remove the hydrogen dissolved in the matrix, dissolve impurities, intermetallic phases and carbides, and increase the homogeneity of the chemical composition of the matrix phase [27–32]

The increase in WHA strength after plastic deformation results from the increase in the dislocation density, occurring especially in the matrix area and increasing the hardness and strength of the alloy. The deformation of the material during plastic working begins with a soft matrix, in which there is a strong increase in the dislocation density, leading to its deformation strengthening. The deformation of the tungsten grains begins only after the matrix has been strengthened sufficiently. The plasticity of WHA depends on the proportion of the matrix, which determines the degree of plastic working that can be obtained. Thus, along with increasing the fraction of tungsten in the alloy, the possibility of its plastic processing decreases. A characteristic feature of the WHA microstructure after plastic working is the elongation of tungsten grains along the rod axis in the direction of plastic working [27–32].

The main aim of the works presented in the article was appropriate optimization of the heat treatment and plastic working processes of the WHA sinters allowing to increase their mechanical properties desired from the application as kinetic energy penetrators point of view.

The ability to penetrate the armor plate by sub-caliber projectile depends on the density of the core material, its shape and strength and plastic parameters. The mechanical parameters of the sub-caliber core must be sufficient to ensure its non-damage from dynamic loads during the initial stage of the shot and passage through the barrel and the required depth of penetration of the armor plate [32–34].

2 Materials and methods

Based on available literature data, performed engineering calculations and available data of currently manufactured WHA materials, the parameters of the expected alloy were determined. To ensure the required penetration depth of the plate, the following parameters of the sub-caliber core made of WHA were adopted: density – 17.4 g/cm^3, tensile strength Rm > 1400 MPa, yield strength $R_p0.2$ > 1350 MPa, elongation, A_5 > 11%, impact strength determined in Charpy impact test according to ISO 148-1, KC > 115 J/cm^2 and hardness > 40HRC. Based on the previously conducted tests published in [26], it was found that the alloy with the composition W91–6Ni–3Co after heat treatment and cold swaging deformation with reduction of 25% complies all the technical required conditions. To produce WHA, the parameters of the sintering process, heat treatment and plastic processing, included in the paper [32], were used. The investigation of the mechanical properties of the tungsten rods was followed at the laboratory of heavy alloys at the Warsaw University of Technology (Poland). At the beginning the powders, W, Ni and Co were bind for 20 h in a drum mixer to achieve adequate homogeneity (Fig. 2) [22].

In the next step, the die pressing of 7.5 kg batches of the mixture was done on the Voehler angle press applying 200 MPa. As a result of the pressing process, rods with dimensions 38 mm in diameter and 550 mm in length were obtained (Fig. 3) [22].

The liquid-phase (LPS) sintering process in a hydrogen atmosphere took 20 min at 1530 °C (Fig. 4) [22].

The rods were then heat-treated to obtain the appropriate plasticity required for cold forming (vacuum chamber at 5 Pa, temperatures 950 °C ÷ 1150 °C, 9 h). The next stage was cold swaging of the WHA rods with reductions of 25% (Fig. 5) [22].

After the forging process, the rods reached their length 520 mm and the diameter 27 mm (Fig. 6).

Then, the manufactured WHA rods were subjected to dimensional tests, post-LPS density, strength parameters and microstructure. The density of the WHA material was measured on a hydro-balance. The quasi-static mechanical properties (R_m, $Rp_{0.2}$, A_5) were determined with Instron 1115 machine. Moreover, by the Charpy drop hammer machine the impact resistance was evaluated. The tests were conducted on standard 10 × 10 ×

Fig. 2 Laboratory mixer

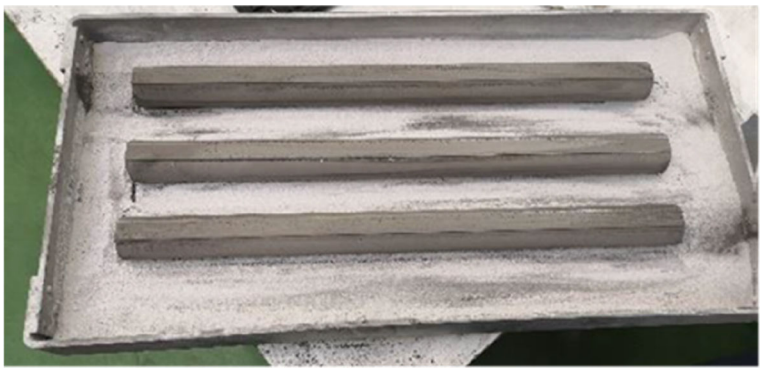

Fig. 3 Mold for pressing tungsten rods

Fig. 4 Sintering of tungsten rods in a chamber furnace

55 mm impact test samples without notches. The Rockwell hardness test was elaborated in a perpendicular plane to the WHA rods axis. The microstructure of the samples was examined by SEM (scanning electron microscope) on polished sections perpendicular and parallel to rod axis in the as-LPS processed condition, after heat treatment as a first stage and after heat treatment with plastic forming as a second stage. For metallographic investigation, the microscope Nikon Eclipse MA200 was used. In addition, some WHA specimens handed over to SEM fractography with LEO 1530 SEM at magnification of 500×, to 5000× [22].

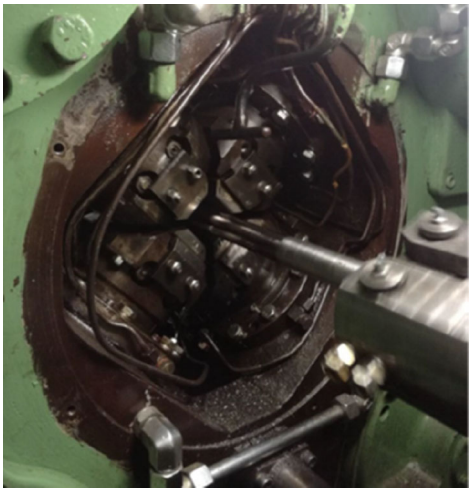

Fig. 5 Cold swaging rods on a radial swaging machine STEYER SPH06.09

Fig. 6 WHA rod after forging

Table 1 Mechanical properties of WHA rods

Machining status	Design mass density [g/cm^3]	Actual mass density [g/cm^3]	Tensile strength, R_m [MPa]	Proof stress, $R_{p0.2}$[MPa]	Unit elongation A_5 [%]	Tensile strength in Charpy test, KC [J/cm^2]
After heat treatment	17.46	17.45 ± 0.01	1155 ± 8	819 ± 5	32 ± 0.8	275 ± 18
After cold swaging reduction 25%			1397 ± 11	1372 ± 9	9.8 ± 1.1	119 ± 21

The microhardness tester machine (Future-Tech FM 810, Future-Tech Corp. Tokyo, Japan) was used to evaluate the microhardness. These tests were elaborated on under a load of 25 g and a dwell time of 15 s. The obtained average results were obtained by 20–25 measurements in a selected area. The HRC hardness tester machine (HR-150A, Jinan Hensgrand Instrument Co., LTD., Jinan, China) was used to hardness test with a standard load.

3 Laboratory tests

3.1 Tests results of mechanical properties

Table 1 presents the results of tests of WHA rods in the condition after heat treatment and plastic working. The presented results of the density measurement show that the actual density of the WHA material is the same as the assumed theoretical density of 17.46 g/cm^3. The use of plastic working causes the tensile strength to be increased by over 200 MPa (from 1155 to 1397 MPa what constitute growth of the tensile strength by 21%) and the yield strength by nearly 500 MPa (from 819 to 1372 MPa what constitute growth of the yield strength by 67%). On the other hand, such significant hardening during plastic working causes a significant decrease in A_5 elongation (from 32 to 9.8% what constitutes 69% drop of the elongation) and KC impact strength in Charpy test by 155 J/cm^2 (from 275 to 119 J / cm^2 what constitute 57% drop of the impact strength).

It should be clarified that the results presented in the current study were the final ones obtained for the alloys subjected to the heat treatment and plastic working processes optimized during previously performed works

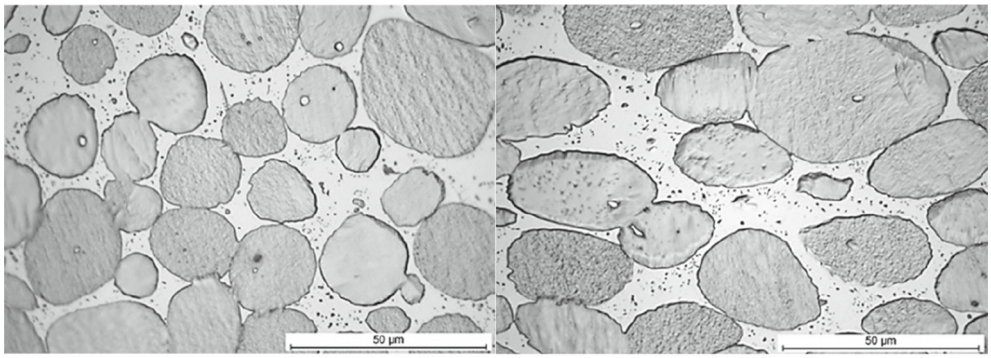

Fig. 7 Microstructure of the WHA rod material heat treatment (**a**) and plastic treatment (**b**)

of the team of the authors [32]. High strength and low plasticity are suitable for the application of these alloys for kinetic projectile penetrators. Tungsten alloys used so far in the production of ammunition had strength parameters lower by about 10%.

3.2 Metallographic examination results

The photographs (Fig. 7) show examples of the microstructures of the WHA rod material made on sections parallel to the longitudinal axis of the rods. Figure 7a shows the microstructure of the WHA rod material after heat treatment, and Fig. 7b shows the microstructure after plastic treatment. Based on the metallographic analysis, it can be concluded that the material in the heat-treated state is homogeneous with correctly shaped (equiaxed) tungsten grains. The tungsten grains are evenly distributed in the W–Ni–Co matrix. There were no defects in the material in the form of bubbles, voids, not properly formed tungsten grains, or larger areas of "pools" of the matrix, which visibly reduce the mechanical parameters of the alloy. In the matrix area, there are small precipitates formed during the heat treatment process. Probably these are phase precipitations of the (Ni, Co) 3W or (Co, Ni) 7W6 type. In the material of the WHA rod after plastic working, the grains are elongated in the direction of the longitudinal axis of the rod (along the direction of plastic working). There were no cracks in the material that could arise during forging and the associated material strengthening process. The average size of the tungsten grains in the material after heat treatment is 24.3 ± 4.8. The elongation of the tungsten grains in the direction of plastic working is 1.6 ± 0.06.

3.3 Fractographic observations

The evaluation of the nature of the fracture (that allows inference about the mode of fracture) was performed by scanning electron microscopy (SEM). The photographs show examples illustrating the typical nature of the fracture surface of WHA rod samples.

Based on the fractographic observation, it can be concluded that the fracture of the WHA rod material in both states is mixed. The photographs presented in Fig. 8 are an example of this type of crack. The characteristic craters visible in the photographs prove the high ductility of the matrix. Next to them, there are transcrystalline cracks along the tungsten cleavage planes, which testify to the high strength at the tungsten–matrix interfaces. In some areas, the presence of the so-called secondary cracks characterized by orientation approximately perpendicular to the scrap surface. The surface of the analyzed fractures is typical for tungsten heavy alloys. No areas were identified where there would be defects in the form of chips or lack of contact between the tungsten grains and the matrix that could initiate the fracture process.

3.4 Hardness and microhardness test results

Tungsten heavy alloys in terms of their microstructure are often treated as two-phase composites containing tungsten grains and a matrix of W–Ni–Co composition. Therefore, the microhardness measurement for both

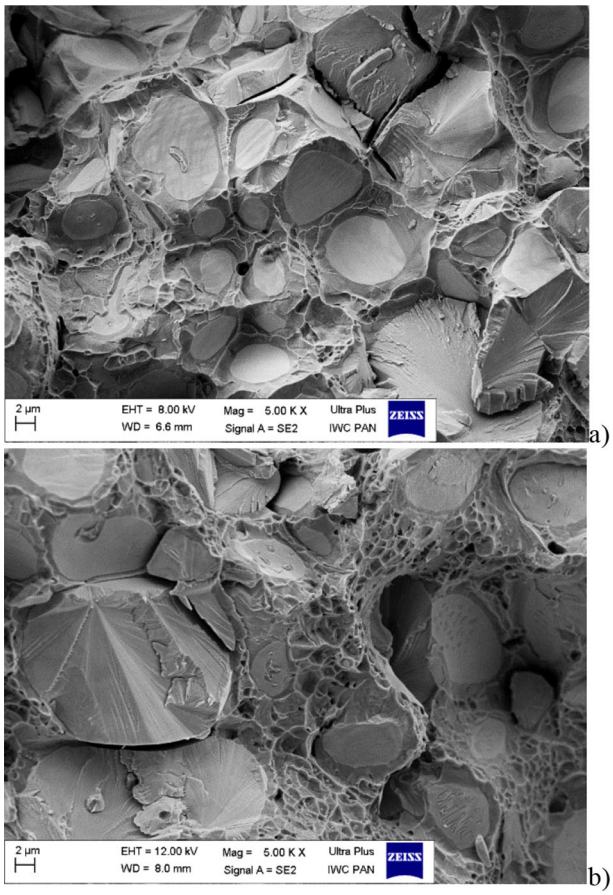

Fig. 8 Examples of typical fractures occurring in a material after heat treatment (**a**) and plastic treatment (**b**)

Table 2 Hardness and microhardness test results

Machining status	Matrix [HV 0.025]	Tungsten grain [HV 0.025]	Hardness [HRC]
After heat treatment	445 ± 15	465 ± 17	34 ± 0.4
After cold swaging reduction 25%	621 ± 30	558 ± 19	46 ± 0.6

phases was taken separately. Table 2 shows the results of measurements of HRC hardness and microhardness HV0.025.

The presented measurement results show the character and degree of hardening of the two phases occurring in the WHA rods. In the condition after heat treatment, the microhardness of tungsten grains (465 HV0.025) is slightly higher than the microhardness of the W–Ni–Co matrix (445 HV0.025). The use of cold working with 25% reduction causes an increase in the microhardness of both the tungsten grains and the matrix. The increase in matrix hardening and the value of its microhardness after plastic treatment is higher than the hardening of tungsten grains. After cold swaging, the matrix microhardness (Fig. 9) is 621 HV 0.025 units (an increase by nearly 180 HV0.025 units compared to the state after heat treatment), and the tungsten grain microhardness is 558 HV0.025 (an increase by over 90 HV 0.025 units). The presented results show that the matrix with the chemical composition of W–Ni–Co shows a greater ability to strengthen during the cold swaging process than chemically pure tungsten grains, which could result in the case of using a higher degree of compression, the formation of transcrystalline cracks through the W grains. Plastic treatment also increases the hardness by 12 HRC units (from 34 to 46 HRC).

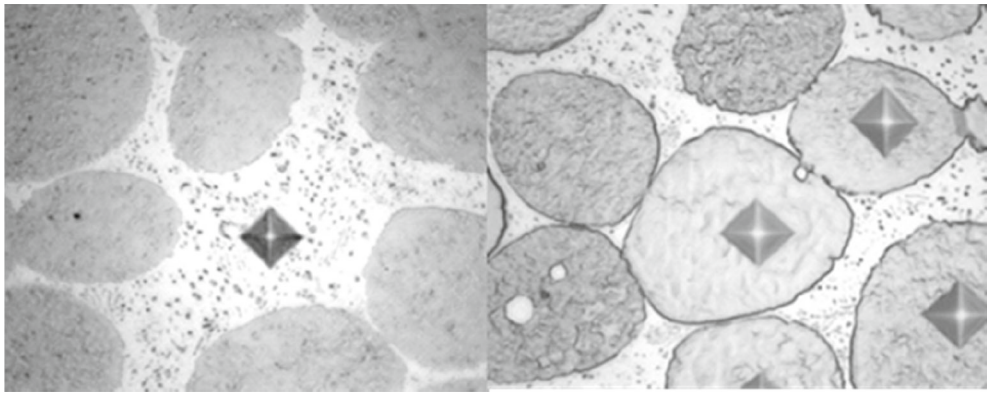

Fig. 9 View of indenter imprints in the matrix and tungsten grains

Fig. 10 120 mm sub-caliber projectiles with new WHA penetrator before loading to gun

4 Results of dynamic tests

The purpose of the research was to check the strength and functioning of the new WHA rods used in 120 mm sub-caliber projectiles. This examination was crucial for the completion of this research work, and its results allowed synthesis of laboratory results and expected implementation. The projectiles equipped with new WHA rods were produced and fixed with propellant charges at the factory MESKO S.A. in Skarżysko-Kamienna, Poland (Fig. 10). It should be indicated that the main aim of the tests was not an evaluation of the penetration capabilities of the alloys but the proper functioning of the projectiles.

The army standard 120 × 570 mm sub-caliber ammunition was used to make the research models. So far, it has had penetrators made of imported rods with a tensile strength lower than 1300 MPa. In the research models, the old penetrators were replaced with newly developed ones made of WHA alloy subjected to optimized heat treatment and plastic working processes.

The tests were conducted by using 120 mm ballistic gun installed on the mounting (Fig. 11) on the firing range of the Military Institute of Armament Technology in Stalowa Wola (Poland).

The ballistic gun was adopted from Leopard 2A4/5 battle tank as equivalent to a combat gun.

The firing tests were conducted at the simultaneous measurements of muzzle velocities of the penetrator with the ballistic radar SL 520. The movement of the projectile leaving the barrel muzzle (V_0, $V_{(x)}$) was registered with the Phantom V710 camera (Fig. 12). Moreover, a set of Kistler piezo-sensors were used to measure the pressure in the gun chamber ($P_{maxpiezo}$).

The use of radar measuring the velocity of the penetrator on the flight path is necessary to assess its correct functioning.

Moreover, the observation through high-speed camera allows to assess the correctness of the separation of the sabots from the penetrator when the projectile leave the barrel.

Fig. 11 120 mm ballistic gun

Fig. 12 A frame from firing a round conditioned at temperature of 233 K

The 16 rounds were fired during the tests. First six rounds were shot at air temperature (the first shot was warm-up shot). The next 10 round were conditioned in temperature chambers for 24 h at the temperatures of − 40 °C (5 rounds) and + 63 °C (5 rounds).

The conditioning temperatures of this type of ammunition are specified in the requirements of national standards [33,34].

The results of the shooting tests are presented in Table 3.

The obtained results of the maximum pressure are characterized by a low standard deviation for individual series of shots. It is required that the standard deviation of the pressure values in the series of shots does not exceed 5% of the P_{maxav} [33,34].

The following standard deviations of the pressure values were obtained for each series: 4.48 MPa (+ 30 °C) − 0.77% P_{maxav}, 8.55 MPa (+ 63 °C) − 1.26% P_{maxav}, 3.61 MPa (− 40 °C) − 0.77% P_{maxav}. Additionally, the maximum allowable pressure of gunpowder gases in the barrel should not exceed 726.3 MPa.

It is similar in the case of the dispersion of muzzle velocity values (V_0). It is required that the standard deviation of the muzzle velocity values in the series of shots does not exceed 5 m/s [27,28]. The following standard deviations of the muzzle velocity values were obtained for each series: 3.72 m/s (+ 30 °C), 4.67 m/s (+ 63 °C), 1.17 m/s (− 40 °C).

The element enabling the verification of the proper functioning of the penetrator on the flight path was a shield plate located at about 1000 m opposite the background of the earth embankment. Based on the holes shape regularity, it was possible to assess the correctness of the penetrator's flight (Fig. 13).

According to obtained results (shapes of holes), it can be assessed that the penetrators moved stably on the flight path, and the yaw angle did not exceed 1° [33,34].

Table 3 Results of the shooting tests

No of shot	Temperature of the round	$P_{max\ piezo}$[MPa]	V_0 [m/s]	$V_{(x)}$ [m/s]	Assessment of strength
1	+ 30 °C	534	1699	$1642_{(880)}$	Correct (warm-up shot)
2		582	1703	$1647_{(923)}$	Correct
3		579	1700	$1646_{(860)}$	Correct
4		585	1702	$1645_{(920)}$	Correct
5		591	1709	$1657_{(860)}$	Correct
6		579	1698	$1639_{(930)}$	Correct
Average	V_{0av} =1701.8 m/s	P_{maxav} = 575 MPa			
7	+ 63 °C	677	1749	$1700_{(770)}$	Correct
8		682	1749	$1687_{(860)}$	Correct
9		672	1751	$1708_{(650)}$	Correct
10		663	1740	$1689_{(800)}$	Correct
11		688	1754	$1705_{(795)}$	Correct
Average	V_{0av} =1748.6 m/s	P_{maxav} = 676.4 MPa			
12	− 40 °C	478	1618	$1565_{(630)}$	Correct
13		470	1618	$1573_{(730)}$	Correct
14		467	1615	$1570_{(565)}$	Correct
15		472	1618	$1562_{(900)}$	Correct
16		471	1617	$1562_{(900)}$	Correct
Average	V_{0av} =1617.2 m/s	P_{maxav} = 471.6 MPa			

Fig. 13 Shield plate located at about 1000 m

5 Conclusions

(1) The selection of the optimized chemical composition of the alloy in conjunction with optimized heat and plastic treatment processes (with 25% cold swaging reduction) allowed to obtain a non-porous WHA material with a density of 17.46 g / cm^3 which exceeded the required (operational requirements) density of 17.4 g/cm^3.
(2) The microstructure of the WHA material is correct with properly formed elliptical tungsten grains evenly distributed in the W–Ni–Co matrix. The modified heat treatment process allowed to increase the strength properties of the W91Ni6Co3 alloy by about 150 MPa in relation to the values obtainable during standard heat treatment.
(3) On the basis of the results obtained and previously performed studies [32], it can be stated that the applied compressive strength value with 25% cold swaging reduction is the optimal value, allowing to increase the tensile strength by 21% (from 1155 ± 8 to 1397 ± 11 MPa -expected min.1400 MPa), yield strength by 67% (from 819 to 1372 MPa- expected min.1350 MPa) and hardness by 35% (from 34 to 46 HRC-expected min.40HRC).
(4) Significant hardening of the WHA alloy after heat treatment and plastic working processes causes a significant decrease in A_5 elongation (from 32 ± 0,8 to 9,8 ± 1,1 % what constitutes 69 % drop of the elongation—expected min.11%) and KC impact strength in Charpy test by 155 J/cm^2 (from 275 ± 18 to 119 ± 21 J / cm^2 what constitute 57% drop of the impact strength—expected 115 J/cm^2). These values are

still larger that minimal required for the proper functioning of the penetrator and achieving of the desired penetration capability of target.

(5) Shooting tests proved the correct functioning of the new high-strength WHA sinter in the sub-caliber kinetic energy projectiles. The functioning of the projectiles fired at extreme operating temperatures does not raise any objections. The values of the muzzle velocity of the projectiles and the pressures of the fired series of rounds meet the requirements defined for this type of ammunition. In the next step, a larger batch of ammunition will be mounted for penetration testing also.

(6) High-density cores of armor-piercing fin-stabilized discarding sabots (APFSDS) projectiles besides the shaped charge jets (SCJ) generated from high-explosive anti-tank (HEAT) warheads [35–39], currently constitute the most serious threat for the armors of main battle tanks (MBT) used by armed forces worldwide. The use of more advanced composite ballistic protection systems based on the ceramic or aramid technologies [40–43] will in the future necessitate further development of kinetic ammunition, for which increasingly higher-strength parameters will be required to achieve better penetration capabilities.

Funding This R&D is supported by the Polish Ministry of Science and High Education—project No DOB-BIO8/05/01/2016.

Declarations

Author contribution MM was involved in conceptualization, methodology, investigation, software and writing—original draft preparation. WJ was responsible for visualization, writing—reviewing and editing and funding acquisition. PS, ZG and PZ carried out investigation, data curation and formal analysis. OG contributed to methodology, formal analysis, resources and data curation. EB participated in writing—reviewing and editing. ZP took part in formal analysis and writing—reviewing and editing. PS assisted in validation, resources, methodology, data curation, visualization and project administration.

Conflict of interest The authors declare no conflicts of interest.

Data availability Data sharing is not applicable to this article.

Institutional review board statement Not applicable.

Informed consent statement Not applicable.

References

1. German, R.M.: Liquid Phase Sintering. Plenum Press, New York (1985)
2. German, R.M.: Thermodynamics of Sintering. Sinter. Adv. Mater. (2010). https://doi.org/10.1533/9781845699949.1.3
3. Skoczylas, P., Gulbinowicz, Z., Goroch, O.: Microstructure and properties of tungsten heavy alloy connections formed during sintering with the participation of the liquid phase. Materials **13**(21), 4965 (2020). https://doi.org/10.3390/ma13214965
4. Skoczylas, P., Kaczorowski, M.: Preliminary study of the rhenium addition on the structure and mechanical properties of tungsten heavy alloy. Materials **14**(23), 7365 (2021). https://doi.org/10.3390/ma14237365
5. Bagchi, T.P., Ghosal, P., Muraleedharan, K., Sarma, B., Maitra, N.: Development of W–Ni–Co heavy alloy system. P/M Sci. Technol. Briefs **2**(4), 21–24 (2000)
6. Das, J., Appa Rao, G., Pabi, S.K.: Microstructure and mechanical properties of tungsten heavy alloys. Mater. Sci. Eng. A **527**(29–30), 7841–7847 (2010). https://doi.org/10.1016/j.msea.2010.08.071
7. Murray, J.L., Bennett, L.H., Baker, H., Massalski, T.B.: Binary Alloy Phase Diagrams. American Society for Metals, Metals Park (1986)
8. Upadhyaya, A.: Processing strategy for consolidating tungsten heavy alloys for ordnance applications. Mater. Chem. Phys. **67**, 101–110 (2001)
9. Giorgio, I., De Angelo, M., Turco, E., Misra, A.: A Biot-Cosserat two-dimensional elastic nonlinear model for a micromorphic medium. Contin. Mech. Thermodyn. **32**(5), 1357–1369 (2020). https://doi.org/10.1007/s00161-019-00848-1
10. Barchiesi, E., Misra, A., Placidi, L., Turco, E.: Granular micromechanics-based identification of isotropic strain gradient parameters for elastic geometrically nonlinear deformations. ZAMM-J. Appl. Math. Mech. /Zeitschrift für Angew. Math. Mech. **101**(11), e202100059 (2021)

11. Turco, E., dell'Isola, F., Misra, A.: A nonlinear Lagrangian particle model for grains assemblies including grain relative rotations. Int. J. Numer. Anal. Methods Geomech. **43**(5), 1051–1079 (2019)
12. La Valle, G.: A new deformation measure for the nonlinear micropolar continuum. Zeitschrift für Angew. Math. Phys. **73**(2), 1–26 (2022)
13. Kezmane, A., Chiaia, B., Kumpyak, O., Maksimov, V., Placidi, L.: 3D modelling of reinforced concrete slab with yielding supports subject to impact load. Eur. J. Environ. Civ. Eng. **21**(7–8), 988–1025 (2017)
14. Magier, M.: The conception of the segmented kinetic energy penetrators for tank guns. J. Appl. Mech. **77**(5), 051802 (2010). https://doi.org/10.1115/1.4001714
15. Magier M.: The numerical optimization of the novel kinetic energy penetrator for tank guns. In 26th International Symposium on Ballistics, Miami 12–16 September (2011), Vol. 2, pp. 1171–1080, DEtech Publications, Inc, USA
16. Motyl, K., Magier, M., Borkowski, J., Zygmunt, B.: Theoretical and experimental research of anti-Tank kinetic penetrator ballistics. Bull. Polish Acad. Sci. Tech. Sci. **65**(3), 399–404 (2017). https://doi.org/10.1515/bpasts-2017-0045
17. Kruszka, L., Magier, M., Zielenkiewicz, M.: Experimental analysis of visco-plastic properties of the aluminium and tungsten alloys by means of Hopkinson bars technique. Appl. Mech. Mater. **566**, 110–115 (2014). https://doi.org/10.4028/www.scientific.net/AMM.566.110
18. Kruszka, L., Magier, M.: Experimental investigations of visco-plastic properties of the aluminium and tungsten alloys used in KE projectiles. EPJ Web Conf. **26**, 05005 (2012). https://doi.org/10.1051/epjconf/20122605005
19. Arora, A. Gopal., Rao, V.: Tungsten heavy alloy for defence applications, materials technology. Adv. Perform. Mater. **19**, 210–215 (2008). https://doi.org/10.1080/10667857.2004.11753087
20. Zhou, M., Needleman, A., Clifton, R.: Finite element simulations of shear localization in plate impact. J. Mech. Phys. Solids **42**(3), 423–458 (1994)
21. Clayton, J.: Dynamic plasticity and fracture in high density polycrystals: constitutive modeling and numerical simulation. J. Mech. Phys. Solids **53**(2), 261–301 (2005)
22. Skoczylas, P., Gulbinowicz, Z., Goroch, O., Barcz, K., Kaczorowski, M.: Research into the production of tungsten heavy alloys with specific mechanical properties. Probl. Mech. Armament Aviat. Saf. Eng. **10**(4), 23–36 (2019). https://doi.org/10.5604/01.3001.0013.6483
23. Kumari, A., Prabhu, G., Sankaranarayana, M., Nandy, T.K.: Effect of solution treatment temperature and cooling rate on the mechanical properties of tungsten heavy alloy. Mater. Sci. Eng. A **688**, 225–236 (2017). https://doi.org/10.1016/j.msea.2017.01.113
24. Ravi Kiran, U., Panchal, A., Prem Kumar, M., Sankaranarayana, M., Nageswara Rao, G.V.S., Nandy, T.K.: Refractory metal alloying: a new method for improving mechanical properties of tungsten heavy alloys. J. Alloys Compd **709**, 609–619 (2017). https://doi.org/10.1016/j.jallcom.2017.03.174
25. Skoczylas, P., Kaczorowski, M.: The influence of cyclic sintering on the structure and mechanical properties of tungsten heavy alloy. Arch. Found. Eng. **16**(4), 131–136 (2016). https://doi.org/10.1515/afe-2016-0097
26. Kaczorowski, M., Skoczylas, P., Krzyńska, A., Kaniewski, J.: The strengthening of weight heavy alloys during heat treatment. Arch. Found. Eng **12**(4), 75–80 (2012). https://doi.org/10.2478/v10266-012-0110-1
27. Ravi Kiran, U., Venkat, S., Rishikesh, B., Iyer, V.K., Sankaranarayana, M., Nandy, T.K.: Effect of tungsten content on microstructure and mechanical properties of swaged tungsten heavy alloys. Mater. Sci. Eng. A **582**, 389–396 (2013). https://doi.org/10.1016/j.msea.2013.06.041
28. Kumari, A., Sankaranarayana, M., Nandy, T.K.: On structure property correlation in high strength tungsten heavy alloys. Int. J. Refract. Metals Hard Mater. **67**, 18–31 (2017). https://doi.org/10.1016/j.ijrmhm.2017.05.002
29. Panchal, A., Nandy, T.K.: Effect of composition, heat treatment and deformation on mechanical properties of tungsten heavy alloys. Mater. Sci. Eng. A **733**, 374–384 (2018). https://doi.org/10.1016/j.msea.2018.07.070
30. Katavić, B., Odanović, Z., Burzić, M.: Investigation of the rotary swaging and heat treatment on the behavior of W- and γ-phases in PM 92.5W–5Ni–2.5Fe–0.26Co heavy alloy. Mater. Sci. Eng. A **492**(1–2), 337–345 (2008). https://doi.org/10.1016/j.msea.2008.05.021
31. Katavic, B., Nikacevic, M., Odanovic, Z.: Effect of cold swaging and heat treatment on properties of the P/M 91W–6Ni-3Co heavy alloy. Sci. Sinter. **40**(3), 319–331 (2008). https://doi.org/10.2298/SOS0803319K
32. Skoczylas, P., Goroch, O., Gulbinowicz, Z., Penkul, A.: The effect of cold swaging of tungsten heavy alloy with the composition W91–6Ni–3Co on the mechanical properties. Materials **14**(23), 7300 (2021). https://doi.org/10.3390/ma14237300
33. NO-13-A235:2006/A1:2021, Amunicja artyleryjska – Naboje 120 × 570 mm do gładkolufowych armat czołgowych – Wymagania, Ministry of National Defence, (2021)
34. NO-13-A513:2006/A2:2021, Amunicja artyleryjska – Naboje 120 × 570 mm do gładkolufowych armat czołgowych – Badania, Ministry of National Defence, (2021)
35. Walters, W.P., Zukas, J.A.: Fundamentals of Shaped Charges. John Wiley & Sons, Hoboken (1989)
36. Lavrentev, M.A.: Cumulative charge and the principles of its operation. Uspekhi Mat. Nauk **12**, 41–56 (1957)
37. Chou, P.C.: The stability of shaped-charge jets. J. Appl. Phys. **48**, 4187e95 (1977)
38. Żochowski, P., WarchołR, Miszczak M., Nita, M., Pankowski, Z., Bajkowski, M.: Experimental and numerical study on the PG-7VM warhead performance against high-hardness armor steel. Materials **14**(11), 3020 (2021). https://doi.org/10.3390/ma14113020
39. Żochowski, P., Warchoł, R.: Experimental and numerical study on the influence of shaped charge liner cavity filing on jet penetration characteristics in steel targets. Def. Technol. **23**, 60–74 (2023). https://doi.org/10.1016/j.dt.2022.09.007
40. Zochowski, P., et al.: Comparison of numerical simulation techniques of ballistic ceramics under projectile impact conditions. Materials **15**(1), 18 (2022). https://doi.org/10.3390/ma15010018
41. Burian, W., et al.: Finite element modeling of ballistic inserts containing aramid fabrics under projectile impact conditions - comparison of methods. Compos. Struct. **294**, 115752 (2022). https://doi.org/10.1016/j.compstruct.2022.115752
42. Kurzawa, A., et al.: Assessment of the impact resistance of a composite material with EN AW-7075 matrix reinforced with α-Al2O3 particles using a 7.62 × 39 mm projectile. Materials **13**, 769 (2020). https://doi.org/10.3390/ma13030769

43. Jamroziak, K., et al.: Analysis of Aramid fabric damage mechanisms as a result of different load speeds. Struct. Integr. **24**, 219–226 (2022). https://doi.org/10.1007/978-3-030-97822-8_25